Nationaal Lucht- en Ruimtevaartlaboratorium

National Aerospace Laboratory NLR

NLR-TP-2001-125

The role of grain size in embrittlement of archaeological silver

R.J.H. Wanhill

NLR-TP-2001-125

The role of grain size in embrittlement of archaeological silver

R.J.H. Wanhill

This report has been prepared as a contribution to the archaeometallurgical literature.

Contents

8 Figures

(38 pages in total)

THE ROLE OF GRAIN SIZE IN EMBRITTLEMENT OF ARCHAEOLOGICAL SILVER

R.J.H. Wanhill

National Aerospace Laboratory NLR, Anthony Fokkerweg 2,
1059 CM Amsterdam, The Netherlands

ABSTRACT

Archaeological silver may be embrittled by long-term corrosion and microstructural changes. The embrittlement of artifacts increases with increasing grain size. This is explained by considering the grain boundary character and models describing the interactions between microcracks, lattice dislocations and grain boundaries. Severely embrittled artifacts are frangible or even friable.

KEYWORDS: ARCHAEOLOGICAL SILVER, EMBRITTLEMENT, GRAIN SIZE, GRAIN BOUNDARIES, CRACKS, SEGREGATION, CORROSION.

INTRODUCTION

Silver is normally ductile and easily fabricated. However, archaeological silver can be very brittle owing to long-term corrosion and microstructural changes (Thompson and Chatterjee 1954; Werner 1965; Ravich 1993; Wanhill *et al.* 1998; Wanhill 2000, 2001). Corrosion-induced embrittlement and microstructurally-induced embrittlement may be independent of each other but can also act synergistically (Wanhill *et al.* 1998; Wanhill 2000, 2001).

Werner (1965) stated that larger grain sizes are a primary cause of silver embrittlement. This is incorrect – or at least imprecise – since large grain size silver is usually ductile, as attested by the successful manufacture of large grained archaeological silver artifacts (Werner 1965; Wanhill *et al.* 1998) and by experiments on silver single crystals (Andrade and Henderson 1951; Rosi 1954). Nevertheless, Werner's observations show that grain size must be an important, albeit secondary, factor for archaeological silver embrittlement.

This report examines in detail the role of grain size in embrittlement of archaeological silver. To do this it is necessary first to "set the scene" by describing the types of embrittlement and the basic concept of grain boundary character. However, the mechanisms – or possible mechanisms – of embrittlement are discussed elsewhere, as are the diagnostic techniques and remedial measures (Wanhill *et al.* 1998; Wanhill 2000, 2001).

TYPES OF EMBRITTLEMENT

Corrosion-induced embrittlement

Archaeological silver undergoes general corrosion, figure 1, which results in a brittle, finely granular surface layer of silver chloride (Gowland 1918; Scott 1996; Wanhill 2000, 2001). This surface corrosion does not affect the remaining metal's integrity, although unfavourable conditions may result in an artifact being completely converted to silver chloride (Gowland 1918).

Even so, some artifacts experience localised corrosion that penetrates the silver and enables embrittlement due to cracking along the corrosion paths (Werner 1965; Ravich 1993; Wanhill *et al.* 1998). Examples are shown in figure 2. Intergranular corrosion can occur in mechanically worked and annealed artifacts. Interdendritic corrosion can occur in castings with essentially as-cast microstructures, i.e. little changed by any subsequent mechanical working or annealing, see Scott (1996). Corrosion along slip lines and deformation twin boundaries can occur in an artifact that has not been annealed after final mechanical working, which includes chased and stamped decorations (Wanhill *et al.* 1998): inside the silver these forms of corrosion can lead to additional corrosion along segregation bands. These bands are the remains, modified by mechanical working and annealing heat-treatments, of solute element segregation (coring) and interdendritic segregation that occurred during solidification of an ingot or cupelled button.

Cracking along the corrosion paths in the silver usually results in irregular fracture surfaces with a finely granular appearance. However, highly localised corrosion along slip lines and deformation twin boundaries results in crystallographic fractures, for example the fractograph in figure 2.

Microstructurally-induced embrittlement

This type of embrittlement is most probably a consequence of long-term low temperature ageing, whereby segregation of an impurity element, or elements, occurs to grain boundaries (Wanhill *et al.* 1998; Wanhill 2000, 2001). Cracking appears to be entirely intergranular, and

examples are shown in figure 3. The cracks are characteristically narrow and sharp (unlike intergranular corrosion, see figure 2) except where grains can become bodily displaced, which is itself a characteristic of severe embrittlement. One such displacement is shown in the SEM fractograph of figure 3.

The grain boundary fracture facets are initially clean. Long-term environmental exposure can cause the facets to become locally corroded where slip lines, deformation twin boundaries and segregation bands intersect the fracture surfaces.

Synergistic embrittlement

Corrosion-induced and microstructurally-induced embrittlement can act synergistically (Wanhill *et al.* 1998; Wanhill 2000, 2001). Figure 4 gives examples of the appearances of synergistic embrittlement. Corrosion along slip lines, deformation twin boundaries and segregation bands can result in cracks under the action of external loads or forces (e.g. crushing pressures during interment) and internal residual stresses due to retained cold-work. These cracks can then initiate fracture along microstructurally embrittled grain boundaries – which may fracture anyway, though less easily – under the action of external loads or forces. In turn, grain boundary fractures expose more slip lines, deformation twins and segregation bands to the environment and therefore increase the opportunities for corrosion.

GRAIN BOUNDARY CHARACTER

Grain boundaries strongly influence the properties of metals and alloys. This was first recognised in the derivation of "laws" describing property-dependence on a length scale, usually the average grain size or diameter, d. Examples are the Herring-Nabarro relationship for the strain rate in creep controlled by lattice diffusion of vacancies, $\dot{\epsilon} \propto d^{-2}$; the Coble relationship for the strain rate in creep controlled by grain boundary diffusion of vacancies, $\dot{\epsilon} \propto d^{-3}$; and the Hall-Petch relationships for plastic yield stress, $\sigma_y \propto d^{-1/2}$, or fracture stress, $\sigma_f \propto d^{-1/2}$ (Herring 1950; Nabarro 1948; Coble 1963; Hall 1951; Petch 1953).

These length scale criteria assume all grain boundaries are similar. However, there is now much evidence that grain boundaries have different properties depending on their character, i.e. their type and structure (Chadwick and Smith 1976; Baluffi 1980; Watanabe 1984, 1993, 1994; Watanabe *et al.* 1980, 1989; Lim and Watanabe 1990).

From the literature and their own research Watanabe (1984, 1993, 1994) and Watanabe *et al.* (1980, 1989) suggested dividing grain boundaries into three character-determined categories: low-angle boundaries with misorientation angles less than 15°, high-angle coincidence boundaries with low Σ coincidence, and high-angle random boundaries. The basic distinguishing property is that low-angle and low Σ coincidence boundaries are low-energy boundaries, while random boundaries are high-energy boundaries.

This distinction between grain boundary types and structures is relevant to microstructurally-induced embrittlement of archaeological silver, for two reasons:

(1)   Most silver artifacts were made using combinations of mechanical working and annealing heat-treatments. The resulting microstructures will have mainly high-angle random grain boundaries, see for example Watanabe (1984) and Watanabe *et al.* (1989). This means the artifacts will contain many grain boundaries susceptible to microstructurally-induced embrittlement, assuming that impurity element segregation has occurred (Wanhill 2001).

(2)   A preponderance of high-angle random grain boundaries makes it reasonable, and indeed compatible with empirical observations (Werner 1965), to consider embrittlement in terms of length scale criteria based on the average grain size or diameter, d.

THE ROLE OF GRAIN SIZE

Archaeological silver may have large grain sizes, more than 0.1 mm, e.g. Werner (1965), Wanhill *et al.* (1998), and Werner's metallograph in figure 2. Large grains are due to the annealing heat-treatments that were usually involved in artifact manufacture. The heat-treatments were more or less uncontrolled, by modern standards, and the metalsmith would likely over-anneal to ensure malleability and ductility during further mechanical working and finishing.

As explained in the introduction to this report, although larger grain sizes are not a primary cause of silver embrittlement, Werner's observations show that grain size must be an important secondary factor. Four reasons can be given. These are discussed in the following sub-sections.

Intergranular corrosion

A large grain size facilitates penetration of intergranular corrosion into an artifact. This is clearly demonstrated by Werner's metallograph in figure 2. The artifact concerned is a severely embrittled Roman cup (Werner 1965) with grain sizes up to 0.4 mm, which is nearly the full thickness.

Impurity element segregation

Microstructurally-induced embrittlement caused by impurity element segregation to grain boundaries is likely to be exacerbated by a larger grain size. This will be explained using the schematics in figure 5, which show two possible dependences of the degree of embrittlement, represented by the fracture stress, σ_f, on impurity element concentration at grain boundaries.

Figure 5a shows a "threshold" concept of embrittlement, for which the fracture stress abruptly drops to a minimum value at a critical impurity concentration C_{cr}. This concept predicts no effect of grain size on embrittlement once C_{cr} is reached. Figure 5b shows a more realistic representation of embrittlement (Thompson and Knott 1993), whereby the fracture stress decreases gradually to a minimum at a critical impurity concentration C_{cr}^*. For this behaviour larger grain sizes can increase embrittlement: larger grains mean less grain boundary area to be embrittled by the impurity elements in an artifact, and hence increased concentrations of impurities at the grain boundaries and increased embrittlement (this assumes that C_{cr}^* is not easily reached).

Microcrack initiation

Embrittlement is manifested by cracking under the action of external loads or forces and internal residual stresses, if present. Cracking begins with *microcracks* smaller than or equal to the grain size. At this size or length scale the average grain size or diameter, d, symbolising a preponderance of high-angle random grain boundaries, is likely to strongly influence crack initiation.

Figures 6-8 depict microcrack models[*] applicable to archaeological silver embrittlement. Appendix A includes the nomenclature and definitions for these models, and Appendix B

---

[*] For mathematical simplicity the models in figures 6 and 8 assume the material to be elastically isotropic and homogeneous. On the scale of individual grains this is incorrect for most metals, including silver (Smithells 1967).

describes the models in mainly non-mathematical detail. The following paragraphs summarise the models:

- Figure 6: model applicable to corrosion-induced embrittlement. Microcracks can develop due to corrosion along slip planes, see figures 2 and 4. The stress intensity factors for the configurations shown in figure 6 are

| 2a < d (Fig. 6a) |

$$k_{II}(sb) = \tau_{app} \sqrt{\pi d / 2} \left(1 - \frac{2\tau_i}{\pi \tau_{app}} \bullet \cos^{-1} \left(\frac{a}{d/2} \right) \right) \qquad (1)$$

| 2a = d (Fig. 6b) |

$$k_{II} = \tau_{app} \sqrt{\pi d / 2} \qquad (2)$$

where $k_{II}(sb)$ and k_{II} describe the intensities of the elastic stress fields at the ends of the partially and fully cracked slip bands when they experience an applied shear stress, τ_{app}, parallel to the crack lengths; and τ_i is the internal shear stress opposing the glide of dislocations ($\leftarrow \top; \perp \rightarrow$ in figure 6a).

If there are multiple slip band cracks like those in figure 4, equation (2) can be modified as follows:

$$k_{II} = \tau_{app} \sqrt{\pi d / 2} \left(\sqrt{\frac{3h}{\pi d}} \bullet \left(\frac{d}{h} + 0.2865 \right) \right) \qquad (3)$$

where h is the perpendicular distance between the cracks.

Equations (1)-(3) are valid for cracks larger than about 1 µm, see Appendix B, section B.2.

- Figure 7: model applicable to corrosion-induced and microstructurally-induced embrittlement, whereby corrosion or impurity element segregation reduce the grain boundary fracture energy, γ_f. The criterion for initiation of a grain boundary microcrack is

$$\tau_{app} - \tau_i \geq \sqrt{\frac{2\pi\mu\gamma_f}{(1-\nu)\,d}} \bullet \frac{1}{\sqrt{F(\theta)}} \qquad (4)$$

where µ is the slip plane shear modulus and ν is Poisson's ratio.

- Figure 8: model applicable to corrosion-induced and synergistic embrittlement, whereby microcracks develop due to corrosion along slip planes and facilitate initiation of microcracks at grain boundaries weakened by corrosion or impurity element segregation. The criteria for initiation of grain boundary microcracks are

$$2a < d \text{ (Fig. 8a)} \qquad \tau_{app} \geq \sqrt{\frac{2\pi\mu\gamma_f}{(1-\nu)\,d}} \bullet \frac{1}{\left(1 - \frac{2\tau_i}{\pi\tau_{app}} \bullet \cos^{-1}\left(\frac{a}{d/2}\right)\right)} \bullet \frac{1}{\sqrt{F(\theta)}} \qquad (5)$$

$$2a = d \text{ (Fig. 8b)} \qquad \tau_{app} \geq \sqrt{\frac{2\pi\mu\gamma_f}{(1-\nu)\,d}} \bullet \frac{1}{\sqrt{F(\theta)}}. \qquad (6)$$

The models make the following general predictions:

(1)   The applied shear stress, τ_{app}, required for a given stress concentration or stress intensity that initiates a grain boundary microcrack decreases with increasing grain size.

(2)   The applied shear stress, τ_{app}, required for initiation of a grain boundary microcrack decreases with decreasing grain boundary fracture energy, γ_f.

The effect of grain size on the ease of microcrack initiation *per se* is very significant, see Appendix B, section B.7 and figure B.8. However, there is an additional effect, already discussed with respect to impurity element segregation: larger grains mean less grain boundary area to be embrittled by a given amount of impurities, leading to decreased γ_f and easier microcrack initiation.

Grain size combined with grain boundary character: frangibility and friability

As discussed above, microcrack initiation along embrittled grain boundaries will be easier if the grain size is large. Furthermore, a preponderance of high-angle random grain boundaries means that archaeological silver artifacts will contain many grain boundaries susceptible to impurity element segregation and hence microstructurally-induced embrittlement, *if it has occurred*.

The combination of large grain size and a preponderance of high-angle random grain boundaries in a microstructurally embrittled artifact means many potential initiation sites for microcracks,

and easy fracture paths for microcracks to become macrocracks. In other words, a large-grained microstructurally embrittled artifact will be frangible, even if there is no damage from corrosion.

Of course, a severely corroded large-grained artifact will be frangible also (Werner 1965). And the combination of a large grain size with synergistic embrittlement is even worse: the artifact becomes friable (Wanhill *et al.* 1998).

CONCLUSIONS

(1)   Embrittlement of archaeological silver may be considered in terms of length scale criteria based on the average grain size or diameter.

(2)   Larger grains increase embrittlement in several ways:
  - by facilitating penetration of intergranular corrosion
  - by enabling increased grain boundary concentrations of impurities causing microstructurally-induced embrittlement
  - by facilitating grain boundary microcrack initiation, which may be involved in corrosion-induced, microstructurally-induced and synergistic embrittlement
  - by providing many potential initiation sites for microcracks and easy fracture paths for microcracks to become macrocracks.

(3)   Severely embrittled artifacts are frangible or even friable.

REFERENCES

Andrade, E.N. da C., and Henderson, C., 1951, The mechanical behaviour of single crystals of certain face-centered cubic metals, Philosophical Transactions of the Royal Society, A244, 177-203.

Baluffi, R.W. (ed.), 1980, Grain Boundary Structure and Kinetics, American Society for Metals (ASM), Metals Park, Ohio, U.S.A.

Barrett, C.S., 1952, Structure of Metals, Second Edition, McGraw-Hill Book Company, Inc., New York, New York, U.S.A.

Bennett, A., 1994, Technical examination and conservation, Chapter 2 in The Sevso Treasure Part One, Journal of Roman Archaeology, Supplementary Series Number Twelve.

Bilby, B.A., Cottrell, A.H., and Swinden, K.H., 1963, The spread of plastic yield from a notch, Proceedings of the Royal Society of London A, 272A, 304-314.

Chadwick, G.A., and Smith, D.A. (eds.), 1976, Grain Boundary Structure and Properties, Academic Press, London, U.K.

Coble, R.L., 1963, A model for boundary diffusion controlled creep in polycrystalline materials, Journal of Applied Physics, 34, 1679-1682.

Cottrell, A.H., 1953, Dislocations and Plastic Flow in Crystals, First Edition, Oxford University Press, London, U.K.

Cottrell, A.H., 1989, Strengths of grain boundaries in pure metals, Materials Science and Technology, 5, 1165-1167.

Coxe, C.D., McDonald, A.S., and Sistare, G.H., Jr., 1979, Properties of silver and silver alloys, in Metals Handbook Ninth Edition, Volume 2 Properties and Selection: Nonferrous Alloys and Pure Metals (Editors W.H. Cubberley *et al*.), 671-678, American Society for Metals (ASM), Metals Park, Ohio, U.S.A.

Das, E.S.P., and Marcinkowski, M.J., 1971, Dislocation behaviour at grain boundaries under heterogeneous shear, Materials Science and Engineering, 8, 189-197.

Das, E.S.P., and Marcinkowski, M.J., 1972, Accommodation of the stress field at a grain boundary under heterogeneous shear by initiation of microcracks, Journal of Applied Physics, 43, 4425-4434.

Frank, F.C., and Read, W.T., Jr., 1950, Multiplication processes for slow moving dislocations, Physical Review, 79, 722-723.

Gowland, W., 1918, Silver in Roman and earlier times: I. Pre-historic and proto-historic times, Archaeologia, 69, 121-160.

Hall, E.O., 1951, The deformation and ageing of mild steel: III discussion of results, Proceedings of the Physical Society of London, B64, 747-753.

Hecker, S.S., Rohr, D.L., and Stein, D.F., 1978, Brittle fracture in iridium, Metallurgical Transactions A, 9A, 481-488.

Herring, C., 1950, Diffusional viscosity of a polycrystalline solid, Journal of Applied Physics, 21, 437-445.

Li, J.C.M., 1961, High-angle tilt boundary - a dislocation core model, Journal of Applied Physics, 32, 525-541.

Lim, L.C., and Watanabe, T., 1990, Fracture toughness and brittle-ductile transition controlled by grain boundary character distribution (GBCD) in polycrystals, Acta Metallurgica et Materialia, 38, 2507-2516.

Murr, L.E., 1975, Interfacial Phenomena in Metals and Alloys, 309-310, Addison-Wesley Publishing Company, Inc., Advanced Book Program, Reading, Massachusetts, U.S.A.

Nabarro, F.R.N., 1948, Deformation of crystals by the motion of single ions, Report of a Conference on the Strength of Solids, 75-90, The Physical Society, London, U.K.

Ohr, S.M., 1985, An electron microscope study of crack tip deformation and its impact on the dislocation theory of fracture, Materials Science and Engineering, 72, 1-35.

Petch, N.J., 1953, The cleavage strength of polycrystals, Journal of the Iron and Steel Institute, 174, 25-28.

Ravich, I.G., 1993, Annealing of brittle archaeological silver: microstructural and technological study, in 10th Triennial Meeting of the International Council of Museums Committee for Conservation, Preprints of the Seminar: August 22/27, 1993, II, 792-795, Washington, D.C., U.S.A.

Rice, J.R., and Thomson, R., 1974, Ductile versus brittle behaviour of crystals, Philosophical Magazine, 29, 73-97.

Rosi, F.D., 1954, Stress-strain characteristics and slip-band formation in metal crystals: effect of crystal orientation, Journal of Metals, 6, 1009-1020.

Scott, D.A., 1996, Technical study of a ceremonial Sican tumi figurine, Archaeometry, 38, 305-311.

Smallman, R.E., 1963, Modern Physical Metallurgy, Second Edition, 170, Butterworths, London, U.K.

Smith, E., and Barnby, J.T., 1967, Crack nucleation in crystalline solids, Metal Science Journal, 1, 56-64.

Smithells, C.J., 1967, Metals Reference Book, Volume 3, Fourth Edition, 708, 709, Butterworths, London, U.K.

Stroh, A.N., 1954, The formation of cracks as a result of plastic flow, Proceedings of the Royal Society of London, Series A, 223, 404-414.

Stroh, A.N., 1957, A theory of the fracture of metals, Advances in Physics, 6, 418-465.

Tada, H., Paris, P.C., and Irwin, G.R., 1973, The Stress Analysis of Cracks Handbook, 14.5, Del Research Corporation, St. Louis, Missouri, U.S.A.

Taira, S., Tanaka, K., and Nakai, Y., 1978, A model of crack tip slip band blocked by grain boundary, Mechanics Research Communications, 5, 375-381.

Tanaka, K., Akiniwa, Y., Nakai, Y., and Wei, R.P., 1986, Modelling of small fatigue crack growth interacting with grain boundary, Engineering Fracture Mechanics, 24, 803-819.

Tanaka, K., and Akiniwa, Y., 1999, Mechanics of small fatigue crack propagation, Small Fatigue Cracks: Mechanics, Mechanisms and Applications (Editors K.S. Ravichandran, R.O. Ritchie and Y. Murakami), 59-71, Elsevier Science Ltd., Oxford, U.K.

Thompson, A.W., and Knott, J.F., 1993, Micromechanisms of brittle fracture, Metallurgical Transactions A, 24A, 523-534.

Thompson, F.C., and Chatterjee, A.K., 1954, The age-embrittlement of silver coins, Studies in Conservation, 1, 115-126.

Wanhill, R.J.H., Steijaert, J.P.H.M., Leenheer, R., and Koens, J.F.W., 1998, Damage assessment and preservation of an Egyptian silver vase (300-200 BC), Archaeometry, 40, 123-137: also NLR Technical Publication NLR TP 95372 L, National Aerospace Laboratory NLR, Amsterdam, The Netherlands.

Wanhill, R.J.H., 2000, Brittle archaeological silver. Identification, restoration and conservation, Materialen, 16, 30-35: also NLR Technical Publication NLR TP 97647 L, National Aerospace Laboratory NLR, Amsterdam, The Netherlands.

Wanhill, R.J.H., 2001, Microstructurally-induced embrittlement of archaeological silver, NLR Technical Publication NLR-TP-2001-032, National Aerospace Laboratory NLR, Amsterdam, The Netherlands.

Watanabe, T., Kitamura, S., and Karashima, S., 1980, Grain boundary hardening and segregation in alpha iron-tin alloy, Acta Metallurgica, 28, 455-463.

Watanabe, T., 1984, An approach to grain boundary design of strong and ductile polycrystals, Res Mechanica, 11, 47-84.

Watanabe, T., Fujii, H., Oikawa, H., and Arai, K.I., 1989, Grain boundaries in rapidly solidified and annealed Fe-6.5 mass % Si polycrystalline ribbons with high ductility, Acta Metallurgica, 37, 941-952.

Watanabe, T., 1993, Grain boundary design and control for high temperature materials, Materials Science and Engineering, A166, 11-28.

Watanabe, T., 1994, The impact of grain boundary character distribution on fracture in polycrystals, Materials Science and Engineering, A176, 39-49.

Werner, A.E., 1965, Two problems in the conservation of antiquities: corroded lead and brittle silver, in Application of Science in Examination of Works of Art (Editor W.J. Young), 96-104, Boston Museum of Fine Arts, Boston, Massachusetts, U.S.A.
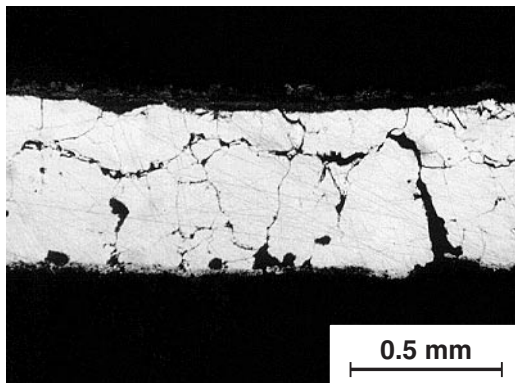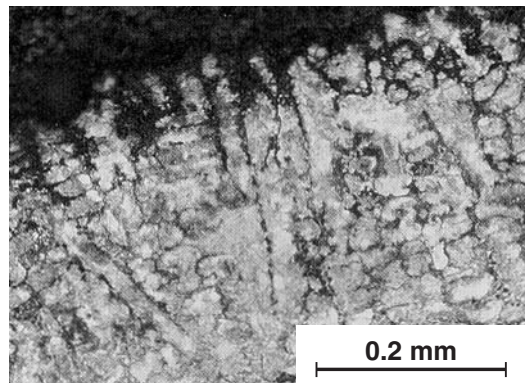
D168-01N
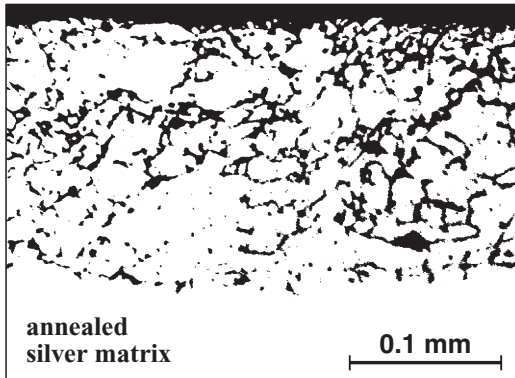
Metallograph (Bennett 1994)
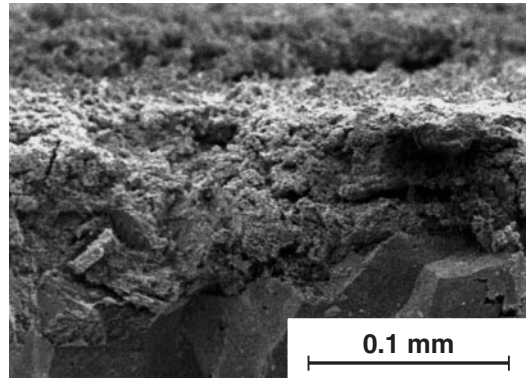
SEM fractograph (Wanhill *et al.* 1995)

Fig. 1 Examples of general corrosion of archaeological silver:
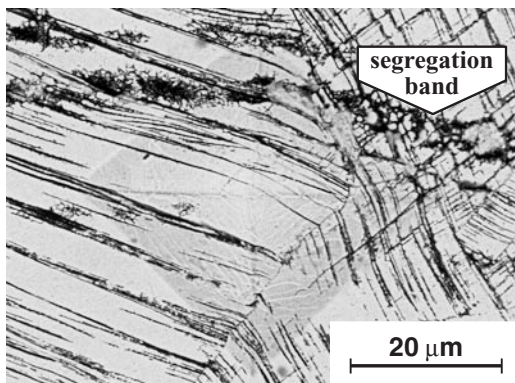SEM = Scanning Electron Microscopy

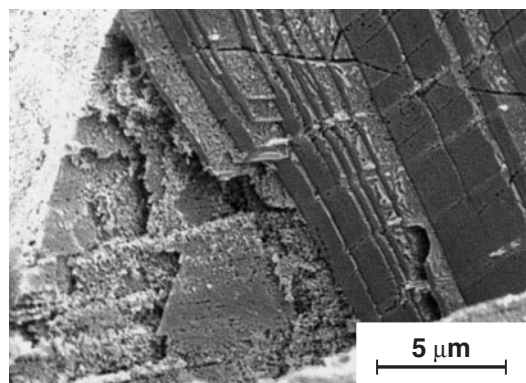Intergranular corrosion: metallograph (Werner 1965)

Interdendritic corrosion: metallograph (Scott 1996)

Slip line, deformation twin boundary and segregation band corrosion

SEM metallograph (Wanhill *et al.* 1998)

SEM fractograph (Wanhill *et al.* 1998)

Fig. 2 Examples of localised corrosion of archaeological silver:
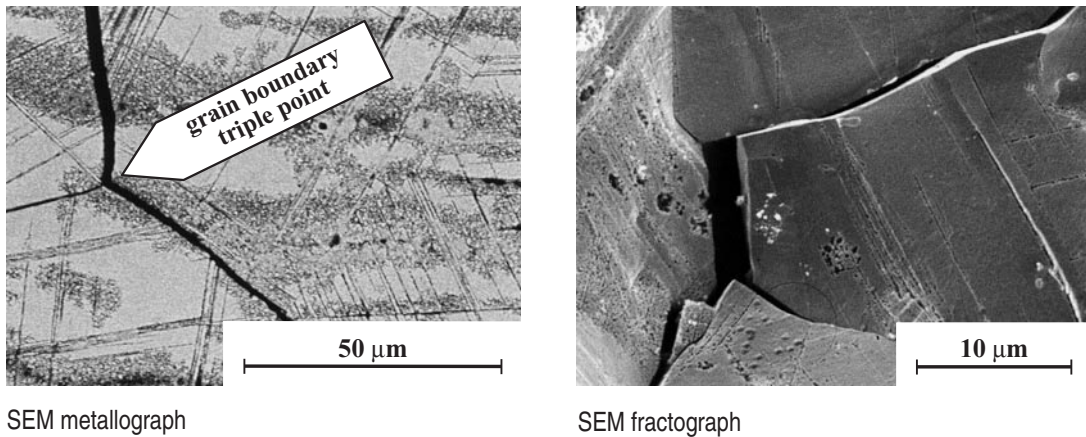SEM = Scanning Electron Microscopy

D168-01N

SEM metallograph

SEM fractograph

Fig. 3   *Microstructurally-induced intergranular fracture in archaeological silver
(*Wanhill *et al.* 1998): SEM = Scanning Electron Microscopy*

Corrosion along slip lines intersecting grain boundary
facets: SEM fractograph (Wanhill *et al.* 1998)

Corrosion along deformation twin boundaries
intersecting a grain boundary facet: SEM fractograph
(Wanhill *et al.* 1998)

Corrosion along segregation bands intersecting grain boundary facets: SEM fractograph (Wanhill *et al.* 1998)
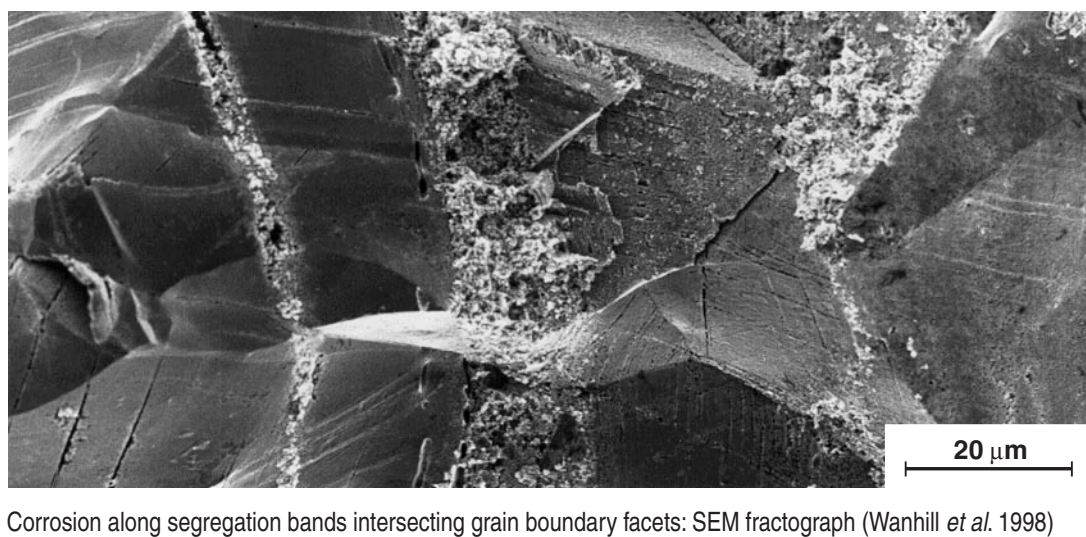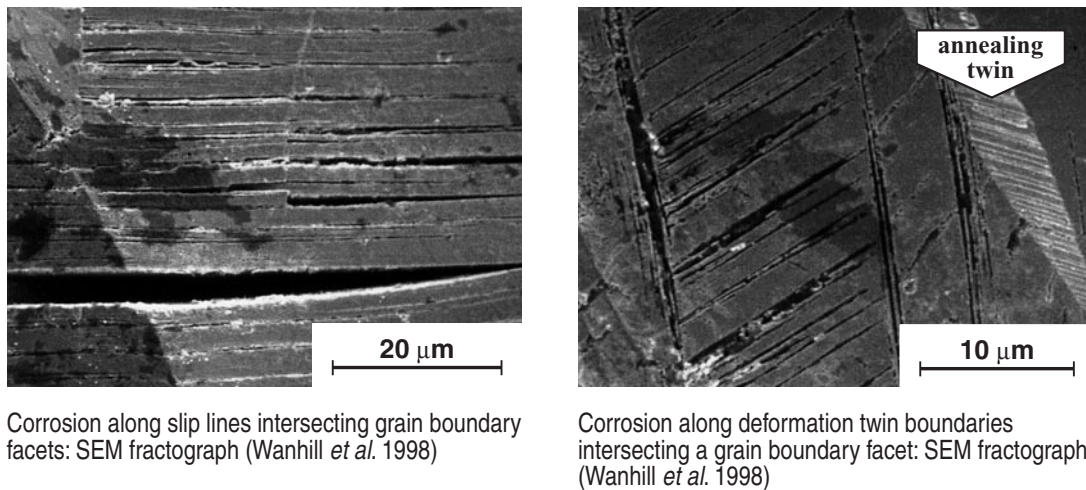
Fig. 4   *Examples of synergistic embrittlement owing to microstructurally-induced
embrittlement (intergranular fracture) and corrosion-induced embrittlement along
slip lines, deformation twin boundaries and segregation bands: SEM = Scanning
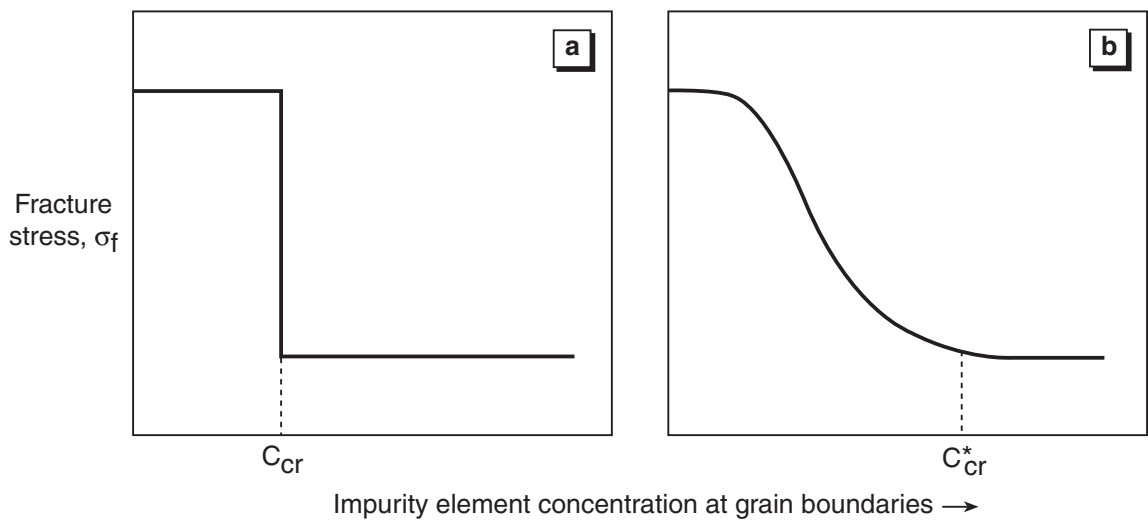Electron Microscopy*

D168-01N

Fig. 5   Dependence of fracture stress, σ_f, on impurity element concentration at grain boundaries:
(a) "threshold" model behaviour in which fracture stress is abruptly lowered at a critical
impurity element concentration, C_{cr}; (b) more realistic behaviour with fracture stress
gradually decreasing to a minimum at a critical impurity element concentration, C^*_{cr}.
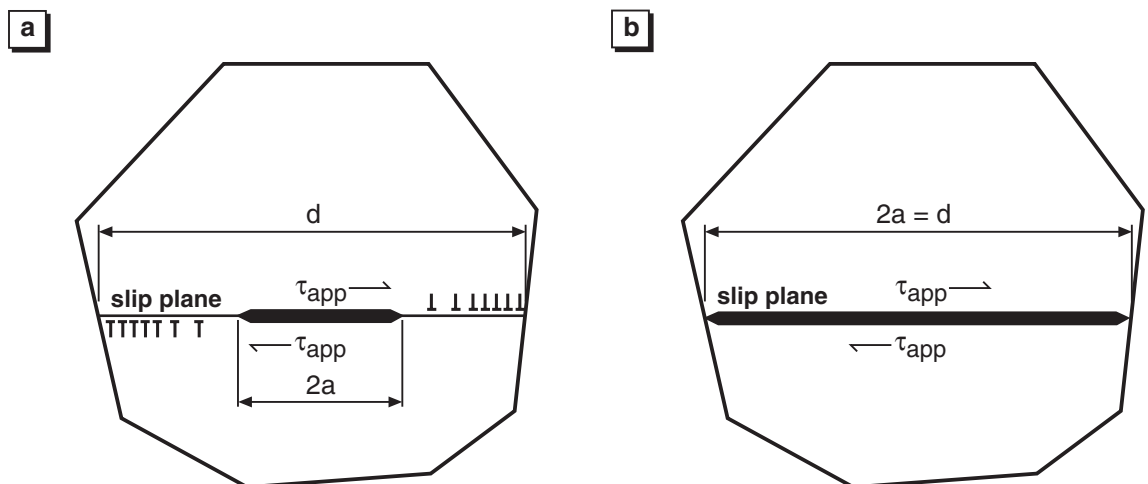After Thompson and Knott (1993)

Fig. 6   Grains containing slip band cracks under mode II shear loading by an applied shear
stress, τ_{app}: (a) crack length 2a less than the grain diameter, d; (b) crack length 2a is
equal to the grain diameter, d. These configurations are applicable to corrosion-induced
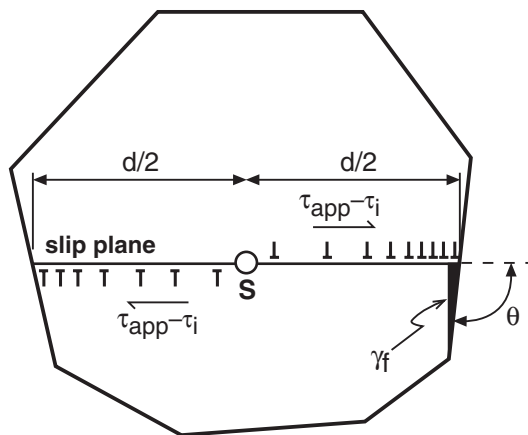embrittlement of archaeological silver

D168-01N

Fig. 7   Grain containing edge dislocation pile-ups at grain boundaries and initiation of a grain
boundary microcrack. The dislocation source, S, emits dislocations under an effective
shear stress, $\tau_{app}-\tau_i$, where τ_{app} is the applied shear stress and τ_i is the internal shear
stress - the back stress - opposing dislocation glide away from the source. γ_f is the grain
boundary fracture energy. This configuration is applicable to corrosion-induced and
microstructurally-induced embrittlement of archaeological silver
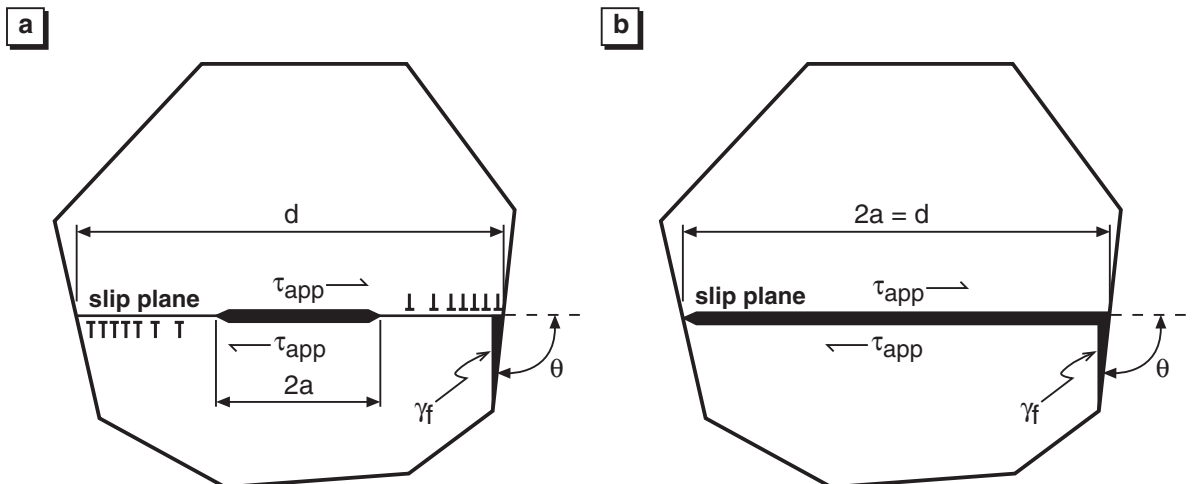

Fig. 8   Grains containing slip band cracks under mode II shear loading by an applied shear stress,
τ_{app}, and initiation of grain boundary microcracks: (a) crack length 2a less than the grain
diameter, d; (b) crack length 2a is equal to the grain diameter, d. These configurations are
applicable to corrosion-induced and synergistic embrittlement of archaeological silver

APPENDIX A: Nomenclature and definitions

a	:	half crack length
α	:	lattice parameter (characterizing interatomic distance in a crystal lattice)
b	:	Burgers vector of a dislocation. Its magnitude and direction specify the distance and direction by which atoms on one side of a slip plane have moved with respect to those on the other side, owing to passage of the dislocation
C_{cr} ; C_{cr}^{*}	:	critical impurity element concentrations at grain boundaries
γ_f	:	grain boundary fracture energy, an elusive and much-debated quantity
d	:	grain size (average grain diameter)
δ	:	interplanar spacing between identical planes in a crystal lattice
e	:	the exponential number, approximately 2.718
$\dot{\varepsilon}$	:	strain rate
$F(\theta), G(\theta)$	:	angular functions, see also θ
h	:	perpendicular distance between parallel slip band cracks
k_{II}	:	stress intensity factor of a crack under shear loading parallel to the crack length direction (mode II loading, also called sliding mode)
$k_{II}^{*}(e)$; $k_{II}(e)$	:	mode II stress intensity factor values required for dislocation emission from the tip of a finite size crack and semi-infinite crack, respectively
$k_{II}(sb)$	:	mode II stress intensity factor for the tip of a slip band
μ	:	shear modulus, an elastic parameter that is constant for isotropic materials
ν	:	Poisson's ratio, an elastic parameter that is constant for isotropic materials
π	:	the well-known transcendental number, approximately 3.142
r_c	:	dislocation core radius, an uncertain quantity
S	:	dislocation source, of which there are several kinds, including cracks, grain boundaries, and dislocations themselves – notably the famous Frank-Read sources (Frank and Read 1950)
σ_f	:	fracture stress (or strength) of a material
σ_y	:	yield stress (or strength) of a material, usually defined as the stress at 0.1 % or 0.2 % offset of the standard stress-strain curve, corresponding to a permanent plastic strain of 0.1 % or 0.2 %
τ_{app}	:	applied shear stress on a slip plane or crack
$\tau_{app}(e)$	:	applied shear stress required for dislocation emission from the tip of a crack

τ_f	:	lattice friction stress (shear stress) opposing dislocation glide along the slip plane; a much debated quantity
τ_i	:	internal shear stress opposing dislocation glide along the slip plane; an indeterminate (variable) quantity
$\tau_{xy}(x)$	:	effective mode II shear stress acting on an edge dislocation gliding along the x-axis
θ	:	angle between a dislocation pile-up and a nucleated crack at the head of the pile-up: see also $F(\theta)$ and $G(\theta)$
x_0 ; x_1	:	distances along the x-axis at which $\tau_{xy}(x) = \tau_f$
$\perp$	:	symbol for an edge dislocation, which is a line discontinuity in the crystal lattice and whose Burgers vector b is perpendicular to the line. The diagram below shows a unit edge dislocation in a simple cubic lattice

extra half plane of atoms

dislocation core
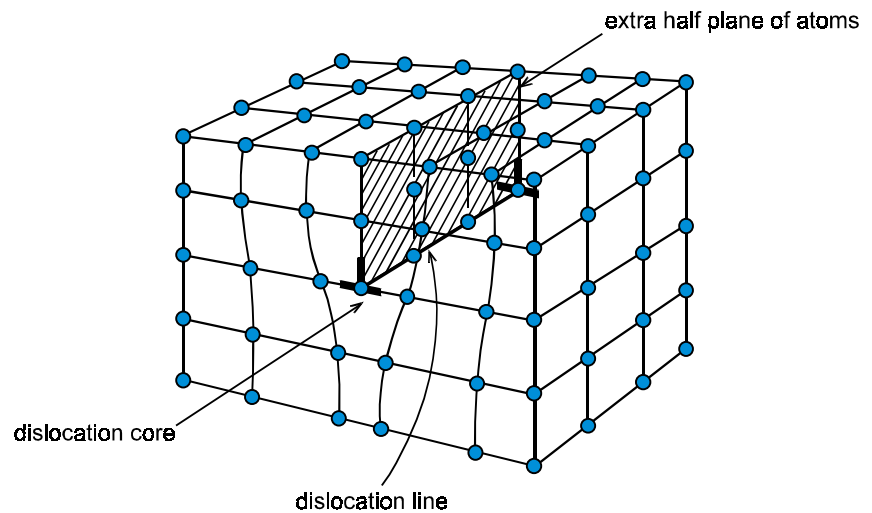
dislocation line

crack stress	:	locally increased stress owing to the presence of a crack
image stress	:	the strain energy of a dislocation decreases when it approaches a free surface, for example a crack tip, because the surface can give way easily to the dislocation's stress field. This means there is a force pulling the dislocation towards the free surface. This force is approximately that expected in an infinite solid between the dislocation and another of opposite sign situated at what would be the position of the dislocation's image on the other side of the free surface. The stress corresponding to this force is called the image stress

slip ; slip planes and slip directions	:	slip is the sliding of one part of a crystal across a neighbouring part. Slip is anisotropic, taking place along certain planes and directions in the crystal lattice, the slip planes and slip directions. Slip actually occurs incrementally, by the passage of numerous dislocations along the slip planes
Σ coincidence	:	grain boundaries can be classified using the concept of a Coincident Site Lattice (CSL). A boundary is then defined according to the ratio of the volume of a unit cell of the CSL to the volume of a unit cell from the grains on either side of the boundary. This ratio is denoted by Σ. A low value of Σ implies many coincident sites (atom positions) per unit area of the boundary. Such boundaries are called low Σ coincidence boundaries

Appendix B: Shear mode crack/dislocation/grain boundary interactions

B.1 Introduction

Rigorous analyses of crack/dislocation/grain boundary interactions require considerable mathematical expertise and knowledge: see for example the classic papers of Stroh (1954), Bilby *et al.* (1963), Smith and Barnby (1967) and Rice and Thomson (1974). However, a generic description and appreciation of the results is less demanding, and is the purpose of this Appendix for the topics germane to the main part of this report.

B.2 Shear mode crack/dislocation interactions for finite length cracks

Analyses of crack/dislocation interactions nearly always assume the crack length to be *effectively* infinite, i.e. the interactions are independent of crack length. The validity of this assumption was examined recently by Tanaka and Akiniwa (1999) for cracks under mode II loading, i.e. shear loading parallel to the crack length direction. Their approach is discussed here.

Consider the situation depicted in figure B.1. Under increasing mode II loading an edge dislocation is emitted from the tip of a sharp crack along the coplanar slip plane (the x-axis). For a crack of length 2a the effective shear stress $\tau_{xy}(x)$ responsible for the glide force on the dislocation along the x-axis is given by

$$\tau_{xy}(x) = \underbrace{\frac{\tau_{app}\,(a+x)}{\sqrt{(a+x)^2 - a^2}}}_{\text{crack stress}} - \underbrace{\frac{\mu b}{2\pi\,(1-\nu)} \bullet \frac{a^2}{[(a+x)^2 - a^2]\,(a+x)}}_{\text{dislocation image stress}} \tag{B1}$$

where τ_{app} is the applied shear stress on the crack; μ is the shear modulus; b is the Burgers vector of the dislocation; π is the well-known transcendental number, approximately 3.142; and ν is Poisson's ratio.

From figure B.1 and equation (B1) it is seen that the effective shear stress acting on the dislocation is the resultant of two opposing stresses, the crack stress and the dislocation image stress. The crack stress tends to drive the dislocation away from the crack tip, while the image stress attracts the dislocation back to the free surface at the crack tip. Figure B.1 and equation (B1) also show the following three important points:

(1) $\tau_{xy}(x)$ is negative very close to the crack tip, because in this region the absolute (negative) value of the image stress is greater than the crack stress. With increasing distance from the crack tip the value of $\tau_{xy}(x)$ becomes less negative and then positive, reaching a maximum and then decreasing gradually to zero.

(2)   Between x_0 and x_1 the value of $\tau_{xy}(x)$ exceeds the lattice friction stress, τ_f, which always opposes dislocation glide along the slip plane.

(3) $\tau_{xy}(x)$ is increased by a greater crack stress, i.e. the first term in equation (B1). This means that at any distance x from the crack tip the value of $\tau_{xy}(x)$ becomes more positive with increasing applied shear stress, τ_{app} .

These three points provide the conditions under which a dislocation can be emitted from the crack tip. Firstly, a dislocation is attracted back to the crack tip in the region $x \le x_0$, as is seen from the $\tau_{xy}(x)$ distribution in figure B.1. Thus for dislocation emission to be possible this "barrier" must be overcome. Rice and Thomson (1974) suggested emission is possible when the crack stress, and hence the value of $\tau_{xy}(x)$, becomes high enough that x_0 decreases to the dislocation core radius, r_c .

Secondly, not only must it be possible for a dislocation to be emitted, but it must also be able to move away from the crack tip. This can happen when $\tau_{xy}(x)$ exceeds τ_f, and the dislocation will then glide to the equilibrium position x_1 .

In short, the criteria for dislocation emission from the crack tip are $x_0 \le r_c$ and $\tau_{xy}(x) \ge \tau_f$. These criteria are combined in the following expression:

$$\tau_{xy}(r_c) \ge \tau_f \tag{B2}$$

From equations (B1) and (B2) we can now state the condition for dislocation emission from the crack tip:

$$\tau_f = \frac{\tau_{app}(e)(a+r_c)}{\sqrt{(a+r_c)^2 - a^2}} - \frac{\mu b}{2\pi(1-\nu)} \bullet \frac{a^2}{[(a+r_c)^2 - a^2](a+r_c)} \tag{B3}$$

where $\tau_{app}(e)$ is the applied shear stress required for dislocation emission.

It is now convenient to introduce the *stress intensity factor* (k) concept. The stress intensity factor is a parameter describing the local elastic stresses ahead of a crack in an isotropic and homogeneous material. The stress intensity factor is useful because it incorporates the applied stress *and* crack length. For a mode II loaded crack the general expression for the stress intensity factor is $k_{II} = \tau_{app} \sqrt{\pi a}$.

Specifically, the mode II stress intensity factor corresponding to dislocation emission from the tip of a crack is given by

$$k_{II}^{*}(e) = \tau_{app}(e) \sqrt{\pi a} \qquad (B4)$$

where $\tau_{app}(e)$ is obtainable from equation (B3).

Equation (B4) has a twofold significance. First, a dislocation can be emitted from the crack tip when the applied stress intensity factor is larger than $k_{II}^{*}(e)$. Second, this condition combines different applied stresses and crack lengths: long cracks with low applied stresses can have the same stress intensity factors as short cracks with high applied stresses.

Equations (B3) and (B4) enable determining $k_{II}^{*}(e)$ for all crack lengths. However, cracks of effectively infinite length have a constant value of $k_{II}^{*}(e) = k_{II}(e)$. The value of $k_{II}(e)$ is obtained by simplifying equation (B3) using the condition $a \gg r_c$, and substituting this simplification into equation (B4). The result is

$$k_{II}(e) = \left(\tau_f + \frac{\mu b}{4\pi r_c \, (1-\nu)} \right) \sqrt{2\pi r_c} \; . \qquad (B5)$$

The last step in this analysis is to use equations (B3)-(B5) to determine the ratio $k_{II}^{*}(e) / k_{II}(e)$ for different crack lengths: the crack length becomes effectively infinite when this ratio first reaches unity. To calculate $k_{II}^{*}(e) / k_{II}(e)$ we need values for μ, ν, b, r_c and τ_f, together with chosen values of half crack length a (or crack length 2a). The values of μ, ν, b, r_c and τ_f are discussed briefly here, before giving the results of the calculation:

- The shear modulus μ is a constant only for isotropic crystals. Like most metals, silver is anisotropic. For polycrystalline silver $\mu \approx 30$ GPa (Smithells 1967). For the slip planes in silver $\mu \approx 20$ GPa (Hecker *et al.* 1978).

- Poisson's ratio ν for silver has been quoted authoritatively as 0.354 (Rice and Thomson 1974) and 0.367 (Smithells 1967).

- The Burgers vector b for unit dislocations on the slip planes in silver is given by $\alpha/\sqrt{2}$ (Smallman 1963), where the lattice parameter $\alpha = 0.40856$ nm (Barrett 1952, 648). Thus b = 0.289 nm.

- The dislocation core radius r_c is taken to be approximately 2b (Rice and Thomson 1974; Tanaka and Akiniwa 1999).

- The lattice friction stress τ_f is a much-debated quantity. A first estimate is obtained from

$$\tau_f = \frac{2\mu}{(1-\nu)} \bullet e^{-\frac{2\pi\delta}{b(1-\nu)}} \qquad (B6)$$

where δ is the interplanar spacing of the slip planes. For silver the slip planes are of {111} type, i.e. their Miller indices are h=k=l=1. From Barrett (1952, 333, 633, 648) we can derive the value of δ : $\delta = \alpha/\sqrt{h^2 + k^2 + l^2} = 0.40856 \text{ nm}/\sqrt{3} = 0.236$ nm.

Equation (B6) was given by Cottrell (1953, 64), who also discussed its limitations, notably that τ_f estimates are much higher than the yield stresses of the softest single crystals. Substitution of the foregoing values of μ, ν, b and δ in equation (B6) gives τ_f estimates ranging from 19-33 MPa. This range is close to the yield stress of annealed polycrystalline silver (Coxe *et al.* 1979), but more than an order of magnitude higher than the yield stresses of silver single crystals, ranging from about 0.5-1.5 MPa (Andrade and Henderson 1951; Rosi 1954).

It might seem that the possible variations in μ, ν and τ_f values, especially the latter, constitute significant problems for the calculation of $k_{II}^*(e)/k_{II}(e)$. However, it turns out that the $k_{II}^*(e)/k_{II}(e)$ ratios are insensitive to variations in μ and ν and large variations in τ_f. This is demonstrated in figure B.2, which plots $k_{II}^*(e)/k_{II}(e)$ versus different crack lengths expressed as the ratio a/r_c.

The main result from figure B.2 is that $k_{II}^*(e)/k_{II}(e)$ reaches unity at $a/r_c \sim 10^3$, in other words a total crack length $2a \sim 1$ μm. This means that mode II loaded cracks more than 1 μm in total length may be considered effectively infinite in size for the purpose of analysing crack/dislocation interactions.

B.3 Shear mode crack/dislocation/grain boundary interactions

Cracks can form along slip planes in metals. Usually this occurs during the early stages of fatigue failure. However, archaeological silver is a special case, whereby slip bands can be partially or wholly converted into cracks by preferential corrosion (Wanhill *et al.* 1998; Wanhill 2000, 2001), see also the main part of this report.

In polycrystalline metals slip band cracks are hindered or arrested by grain boundaries. This phenomenon, which has great practical importance, has been analysed using dislocation theory (Taira *et al.* 1978; Tanaka *et al.* 1986) albeit with the simplification that dislocation-free zones at the crack tips and grain boundaries were neglected (Tanaka and Akiniwa 1999).

Consider the two basic situations depicted in figure B.3. These represent slip band cracks under mode II loading that are contained within a grain. Figure B.3a shows a crack whose length 2a is less than the grain diameter d, together with edge dislocations along the coplanar slip plane. The dislocations ahead of each crack tip are of opposite sign (⊥ as opposed to ⊤), corresponding to the opposing directions of the applied shear stress τ_{app}, and are shown *piled up* against the grain boundaries. Figure B.3b shows a crack that has grown right across the grain, i.e. 2a = d.

Analysis of these two basic situations assumes the material to be isotropic and homogeneous and makes use of the fact that the local elastic stresses ahead of a slip band or crack depend in the same way on the distance from the tip of the slip band or crack (Tanaka *et al.* 1986). These assumptions and condition enable use of the stress intensity factor (k) concept to describe these situations. From Tanaka *et al.* (1986) we can derive the following expressions:

$$
\boxed{\begin{array}{c} 2a < d \\ (\text{Fig. B.3a}) \end{array}} \qquad k_{II}(sb) = \tau_{app}\,\sqrt{\pi d/2}\left(1 - \frac{2\tau_i}{\pi\tau_{app}} \bullet \cos^{-1}\left(\frac{a}{d/2}\right)\right) \tag{B7}
$$

$$
\boxed{\begin{array}{c} 2a = d \\ (\text{Fig. B.3b}) \end{array}} \qquad k_{II} = \tau_{app}\,\sqrt{\pi a} = \tau_{app}\,\sqrt{\pi d/2} \tag{B8}
$$

where $k_{II}(sb)$ and k_{II} are the respective mode II stress intensity factors for the partially cracked slip band in figure B.3a and the fully cracked slip band in figure B.3b; τ_{app}, π, a and d are as defined earlier; and τ_i is the internal shear stress opposing dislocation glide along the slip plane and away from the crack tips. τ_i is a "catch-all" for various obstacles to dislocation glide, see Cottrell (1953, 103-104, 111-112), and in the present case represents mostly the *back stress* caused by dislocations piling up at the grain boundaries, figure B.3a[*].

---

[*] τ_i is often taken to be τ_f, the lattice friction stress. This adds unnecessary imprecision to τ_f, which is really only a component of τ_i.

The main result from equations (B7) and (B8) is that the stress intensity factors $k_{II}(sb)$ and k_{II} show a direct dependence on the grain size, expressed as the square root of half the grain diameter, $\sqrt{d/2}$. In other words, $k_{II}(sb)$ and k_{II} increase with increasing grain size.

B.4 Shear mode dislocation/grain boundary/crack interactions

Here we consider two situations for an *uncracked* slip band subjected to an increasing applied shear stress. Figure B.4 depicts these situations, which are described as follows:

(1)   The left-hand side of figure B.4 represents what generally occurs in polycrystalline metals. Under an applied shear stress, τ_{app}, dislocations are emitted from a source, S. The dislocations glide along the slip plane and pile up against a grain boundary, resulting in a stress concentration at the head of the pile-up. An increase in the applied shear stress causes more dislocations to be emitted and pile up. Eventually the stress concentration at the head of the pile-up becomes high enough to activate a dislocation source, and hence slip, in the neighbouring grain. In this way slip can spread from grain to grain in a polycrystalline metal.

(2)   The right-hand side of figure B.4 shows what can occur when a metal has relatively weak grain boundaries[*], as is possible for archaeological silver (Wanhill *et al.* 1998; Wanhill 2000, 2001). Under the same applied shear stress, τ_{app}, dislocations are emitted from the source, S, and *at first* pile up against a weak grain boundary. However, with increasing applied shear stress the stress concentration at the head of the pile-up causes microcrack initiation along the grain boundary.

Stroh (1954, 1957) and Smith and Barnby (1967) analysed situation (2) with the trivial difference, *from an analytical viewpoint*, that the microcrack need not initiate along a grain boundary. Similarly, Smith and Barnby combined situations (1) and (2), i.e. they analysed the total configuration depicted in figure B.4 without requiring the microcrack to initiate along a grain boundary. Using this analysis we obtain the following criteria for initiation of a grain boundary microcrack:

---

[*] The strength of grain boundaries in metals is somewhat controversial, see Cottrell (1989). Be that as it may, archaeological silver can have grain boundaries seriously weakened by corrosion (corrosion-induced embrittlement) and impurity element segregation (microstructurally-induced embrittlement), as discussed in the main part of this report.

| complete analysis | $\tau_{app} - \tau_i \geq \sqrt{\dfrac{2\pi\mu\gamma_f}{(1-\nu)\,d}} \bullet \dfrac{1}{\sqrt{F(\theta)}}$ | (B9a) |
| analysis neglecting effect of local stresses due to the dislocation pile-up | $\tau_{app} - \tau_i \geq \sqrt{\dfrac{2\pi\mu\gamma_f}{(1-\nu)\,d}} \bullet \dfrac{1}{\sqrt{G(\theta)}}$ | (B9b) |

where τ_{app}, τ_i, π, μ and d are as defined earlier; γ_f is the grain boundary fracture energy; and $F(\theta)$ and $G(\theta)$ are angular functions given by

$$F(\theta) = \frac{1}{4}(5 + 2\cos\theta - 3\cos^2\theta) \tag{B10a}$$

$$G(\theta) = \frac{9}{4}(\sin^2\theta \cos^2\frac{\theta}{2}) \tag{B10b}$$

There are two main results obtainable from equations (B9) and (B10). The more important result is that the effective shear stress, τ_{app}-τ_i, required for grain boundary microcrack initiation depends inversely on the grain size, which is expressed as the inverse square root of the grain diameter, $\sqrt{1/d}$, in equations (B9). In other words, microcrack initiation becomes easier with increasing grain size.

The second main result concerns $F(\theta)$ and $G(\theta)$. Figure B.5 depicts the inverse square roots of these functions, as in equations (B9), for a wide range of θ. From the complete analysis $F(\theta)$ shows the criterion for microcrack initiation is nearly independent of the angle between the slip plane and grain boundary for $0 < \theta < 90°$. However, from the analysis neglecting local shear stresses due to the dislocation pile-up the function $G(\theta)$ provides only a narrow range of θ favourable to microcrack initiation.

This difference between $F(\theta)$ and $G(\theta)$ demonstrates the need to account for local shear stresses. Although this might seem obvious, with hindsight, it is emphasized here because Stroh's analyses (Stroh 1954, 1957) did not include local shear stresses, and his results – notably the narrow range of θ favourable to microcrack initiation – are often quoted without further appraisal.

B.5 Shear mode crack/grain boundary interactions

Figure B.6 depicts two situations derived from those in figures B.3 and B.4, whereby partly or wholly cracked slip bands result in microcrack initiation at relatively weak grain boundaries. As discussed in the main part of this report, for archaeological silver these situations represent either:

(1)   Corrosion-induced embrittlement, with the slip band cracks and grain boundary weakness caused by preferential corrosion.

(2)   Synergistic embrittlement, where the slip band cracks are caused by preferential corrosion and the grain boundary weakness is due to impurity element segregation, i.e. microstructurally-induced embrittlement.

With the knowledge that a slip band crack under mode II loading is equivalent to a pile-up of edge dislocations, except that over the length of a slip band crack the applied shear stress, τ_{app}, is not opposed by an internal shear stress, τ_i, we can substitute equations (B7) and (B8)[*] into equation (B9a) to obtain the following criteria for initiation of a grain boundary microcrack:

$$\boxed{\begin{array}{c} 2a < d \\ (\text{Fig. B.6a}) \end{array}} \qquad \tau_{app} \geq \sqrt{\frac{2\pi\mu\gamma_f}{(1-\nu)\,d}} \bullet \frac{1}{\left(1 - \dfrac{2\tau_i}{\pi\tau_{app}} \bullet \cos^{-1}\left(\dfrac{a}{d/2}\right)\right)} \bullet \frac{1}{\sqrt{F(\theta)}} \qquad (B11)$$

$$\boxed{\begin{array}{c} 2a = d \\ (\text{Fig. B.6b}) \end{array}} \qquad \tau_{app} \geq \sqrt{\frac{2\pi\mu\gamma_f}{(1-\nu)\,d}} \bullet \frac{1}{\sqrt{F(\theta)}}\ . \qquad (B12)$$

where all the parameters are as defined previously.

---

[*] As before, see appendix B.3, the material is assumed to be isotropic and homogeneous.

The main result from equations (B11)[*] and (B12) is that the applied shear stress, τ_{app}, required for grain boundary microcrack initiation depends inversely on the grain diameter, d, in the first square root expression. This indicates that microcrack initiation becomes easier with increasing grain size.

B.6 Multiple shear mode crack/grain boundary interactions

Figure B.7 shows a situation similar to that in figure B.3b, but for two or more slip band cracks separated by a distance h. For this situation we modify equation (B8) with an approximation derived from Tada *et al.* (1973):

$$k_{II} = \tau_{app} \sqrt{\pi a} \left(\sqrt{\frac{3h}{2\pi a}} \bullet \left(\frac{2a}{h} + 0.2865 \right) \right) \tag{B13a}$$

$$= \tau_{app} \sqrt{\pi d / 2} \left(\sqrt{\frac{3h}{\pi d}} \bullet \left(\frac{d}{h} + 0.2865 \right) \right) \tag{B13b}$$

where τ_{app}, π, a and d are as defined earlier.

The main result from equations (B13) is the same as that from equation (B8), namely the stress intensity factor k_{II} shows a direct dependence on the grain size, expressed as the square root of half the grain diameter, $\sqrt{d/2}$. In other words, k_{II} increases with increasing grain size. In addition, k_{II} increases with decreasing distance, h, between the cracks.

B.7 Summary

For crack lengths beyond about 1 μm equations (B7)-(B13) provide *first approximation* analytical description of shear mode crack/dislocation/grain boundary interactions in embrittled archaeological silver; whereby the angular function F(θ) should be used instead of G(θ) for equations (B9), (B11) and (B12).

---

[*] Equation (B11) contains a minor complication. The second expression is a compensating factor, whereby the applied shear stress, τ_{app}, required for grain boundary microcrack initiation is *increased* by an increase in grain diameter, d. However, this compensating factor reflects only the transition from a total slip band crack, 2a = d, to a dislocation pile-up of total length d, and a concomitant change in the required shear stress from τ_{app} to τ_{app}-τ_i, compare equations (B9a) and (B11). In both cases there is the basic dependence of the required shear stress on the inverse square root of the grain diameter, $\sqrt{1/d}$.

These analytical descriptions have limitations. They neglect features such as grain boundary ledges, which are powerful concentrators of stress and strain (Li 1961; Das and Marcinkowski 1971), and dislocation-free zones near crack tips and grain boundaries (Ohr 1985; Tanaka *et al.* 1986). Also, they cannot be fully quantified, since the values of internal shear stress, τ_i, and grain boundary fracture energy, γ_f, are variable or unknown.

On the other hand, grain boundary ledges are produced by dislocation pile-ups (Das and Marcinkowski 1971, 1972; Murr 1975); dislocation-free zones near crack tips are highly localised and *generically* neglectable, see Ohr (1985) and Tanaka and Akiniwa (1999); and for the main part of this report it is sufficient to show the general analytical result that microcrack initiation in embrittled archaeological silver becomes easier with increasing grain size.

In fact, and as an illustration, we can quantify the general analytical result very easily for the situation shown in figure B.6b and represented by equation (B12). From this expression figure B.8 directly plots ratios of applied shear stress, τ_{app2}/τ_{app1}, versus the ratios of average grain diameter, d_2/d_1. If we assume small and large grain sizes in archaeological silver to be represented by d_1 = 5-10 μm and d_2 = 100-200 μm, respectively, then the applied shear stress required for microcrack initiation in the large-grained silver is only 1/3-1/6 that for the fine-grained silver. Thus the effect of grain size on the ease of microcrack initiation is very significant.
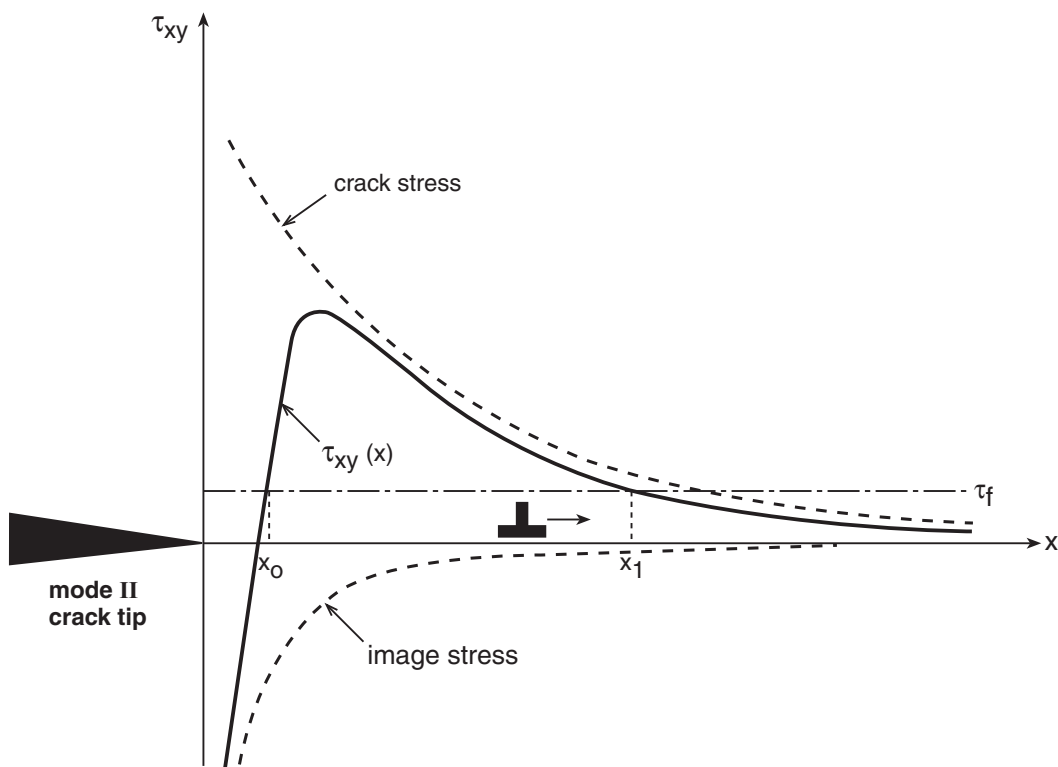
D168-01N

Fig. B.1 Schematic of the stress on an edge dislocation emitted from the tip of a sharp mode II
crack along the coplanar slip plane. The effective shear stress, $\tau_{xy}(x)$, is obtained by
adding the shear stress due to the crack and the dislocation image stress. The dislocation
can glide in the x-direction if $\tau_{xy}(x)$ is greater than the lattice friction stress, τ_f.
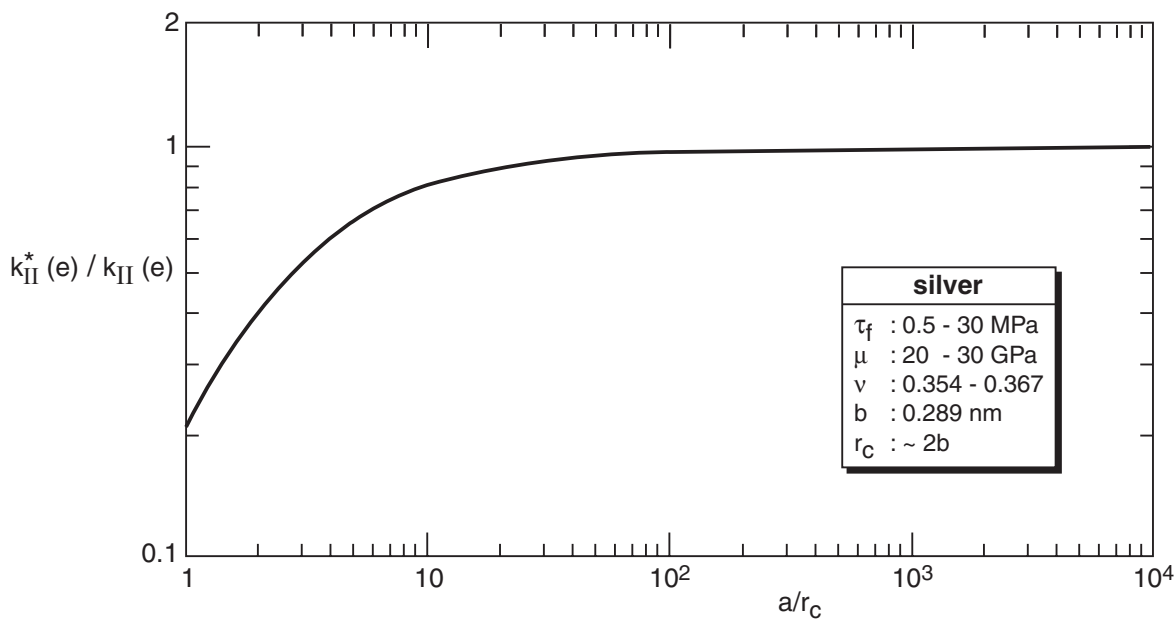This schematic is a modification of one given by Ohr (1985)

Fig. B.2 Dimensionless plot of the mode II stress intensity factors required for emission of edge
dislocations from the tips of finite length cracks

D168-01N
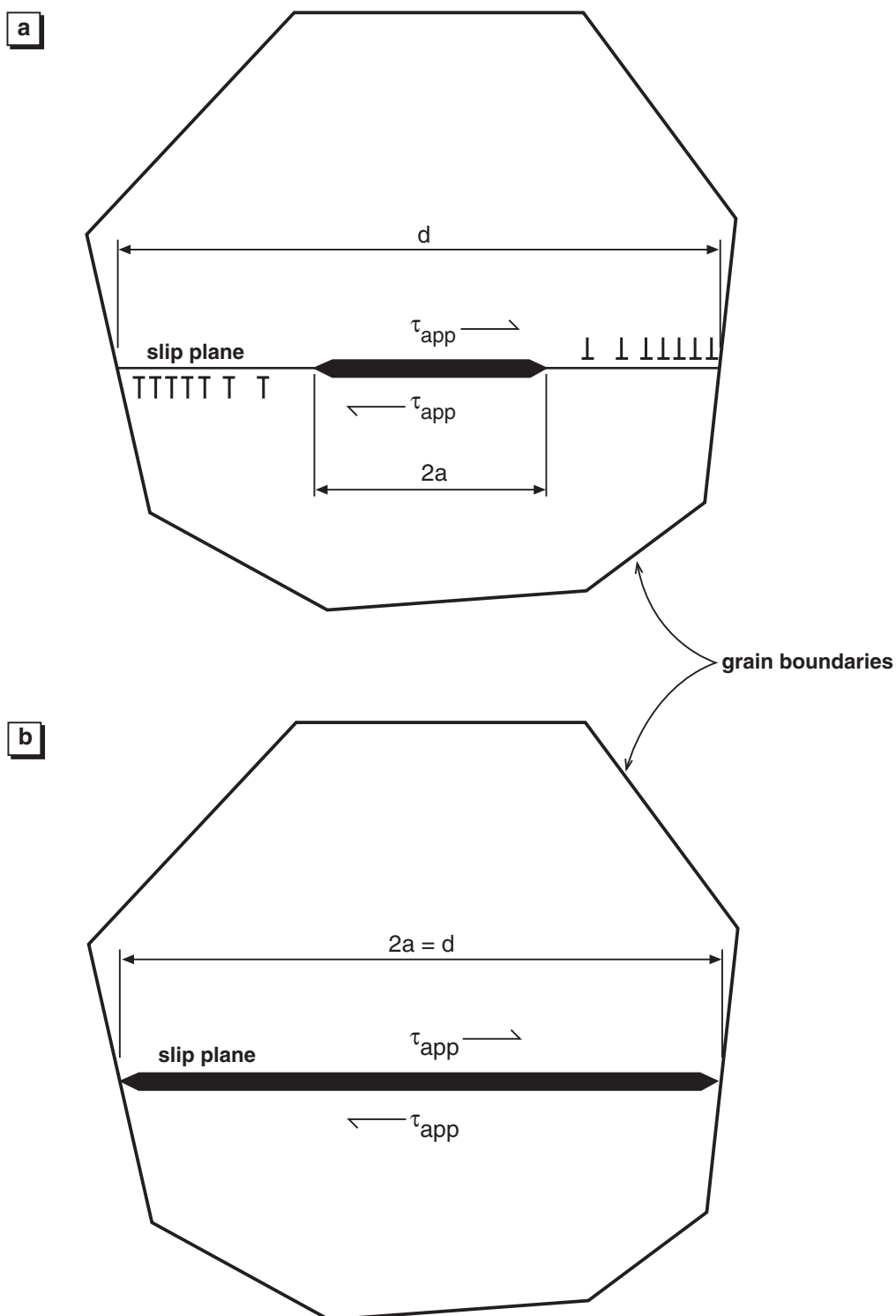
Fig. B.3   Schematics of grains containing slip band cracks under mode II shear loading by
an applied shear stress, τ_{app}: (a) crack length 2a less than the grain diameter, d;
(b) crack length 2a is equal to the grain diameter, d. These configurations are
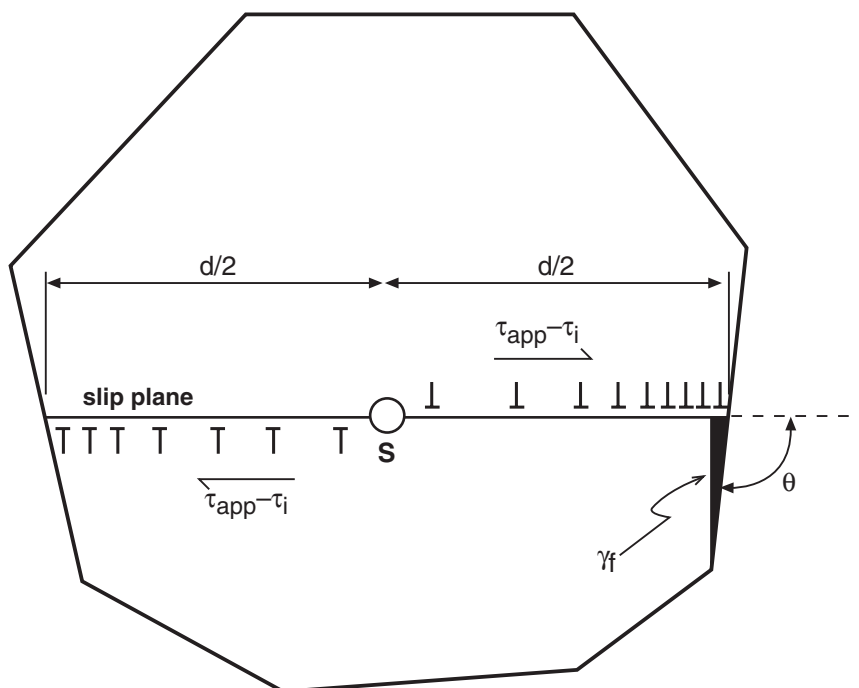applicable to corrosion-induced embrittlement of archaeological silver

D168-01N

Fig. B.4   Schematic of a grain containing edge dislocation pile-ups at grain boundaries and
initiation of a grain boundary microcrack. The dislocation source, S, emits dislocations
under an effective shear stress, $\tau_{app}-\tau_i$, where τ_{app} is the applied shear stress and τ_i is
the internal shear stress - the back stress - opposing dislocation glide away from the
source. γ_f is the grain boundary fracture energy. This configuration is applicable to
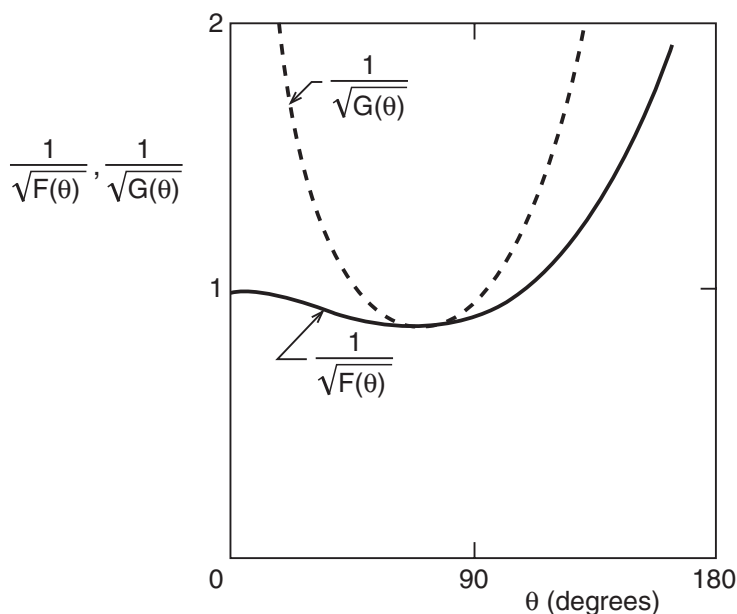corrosion-induced and microstructurally-induced embrittlement of archaeological silver

Fig. B.5   Inverse square roots of the angular functions $F(\theta)$ and $G(\theta)$ derived by Smith and
Barnby (1967). $F(\theta)$ is for a complete analysis of microcrack initiation ahead of an
edge dislocation pile-up, see figure B.4. $G(\theta)$ is for the same analysis but neglecting
local shear stresses due to the pile-up

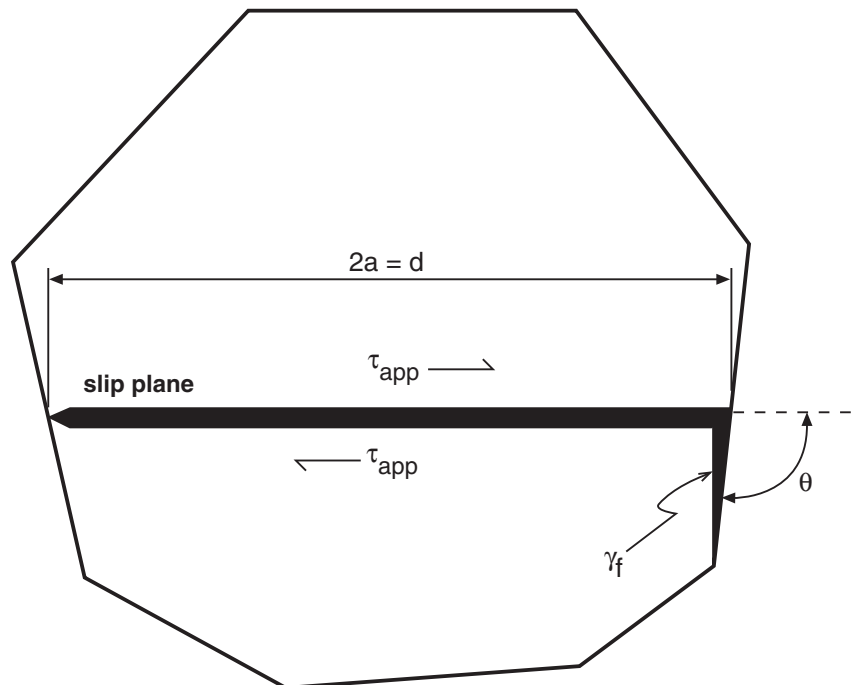D168-01N

a

d

τ_{app} ⟶

slip plane

τ_{app}

2a

γ_f

θ

b

2a = d

τ_{app} ⟶

slip plane

τ_{app}

θ

γ_f
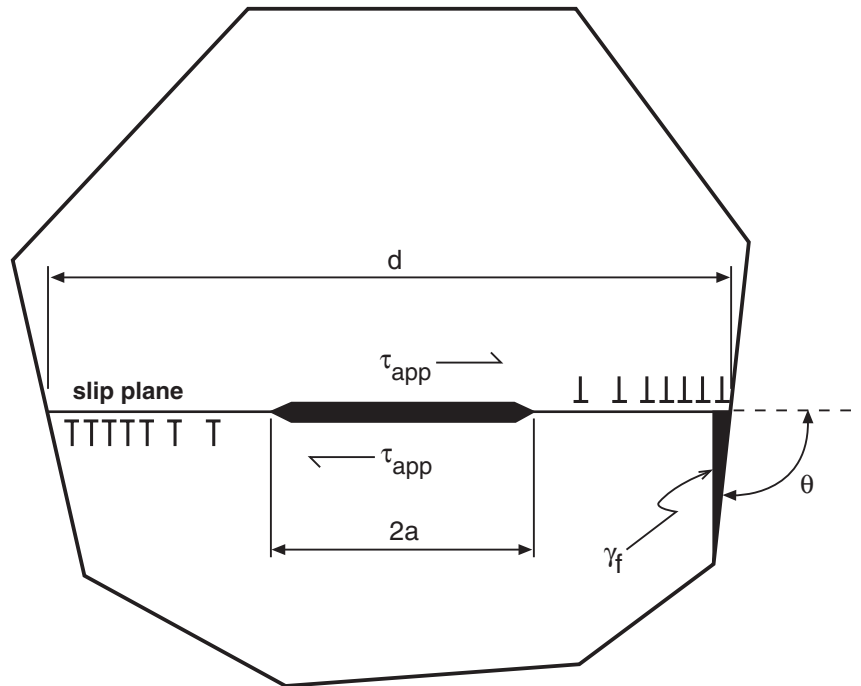
Fig. B.6   *Schematics of grains containing slip band cracks under mode II shear loading by an applied shear stress, τ_{app}, and initiation of grain boundary microcracks: (a) crack length 2a less than the grain diameter, d; (b) crack length 2a is equal to the grain diameter, d. These configurations are applicable to corrosion-induced and synergistic embrittlement of archaeological silver*
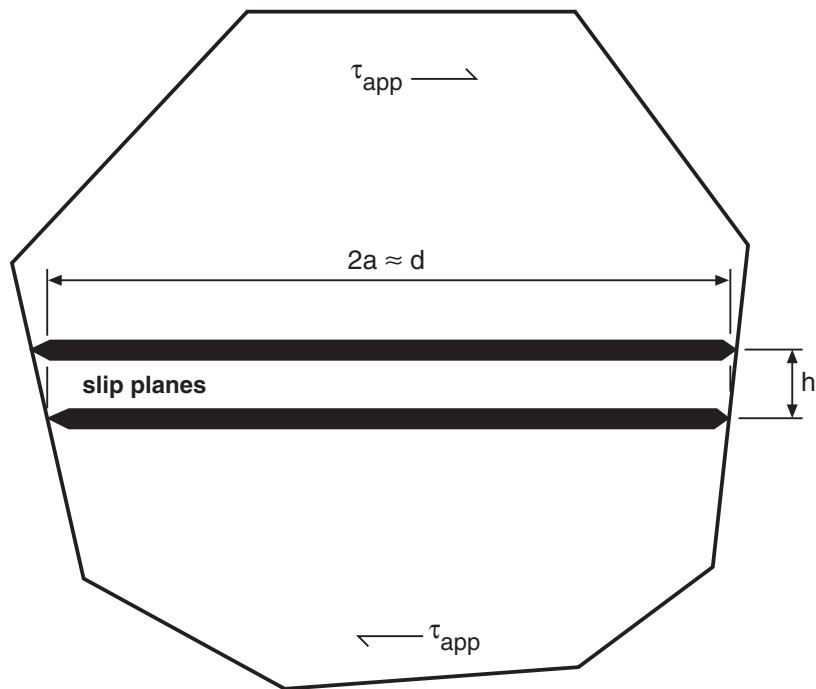
D168-01N

Fig. B.7   Schematic of a grain containing multiple slip band cracks under mode II shear loading by an applied shear stress, τ_{app}. This configuration is applicable to corrosion-induced embrittlement of archaeological silver, and is a modification of the configuration in figure B.3b
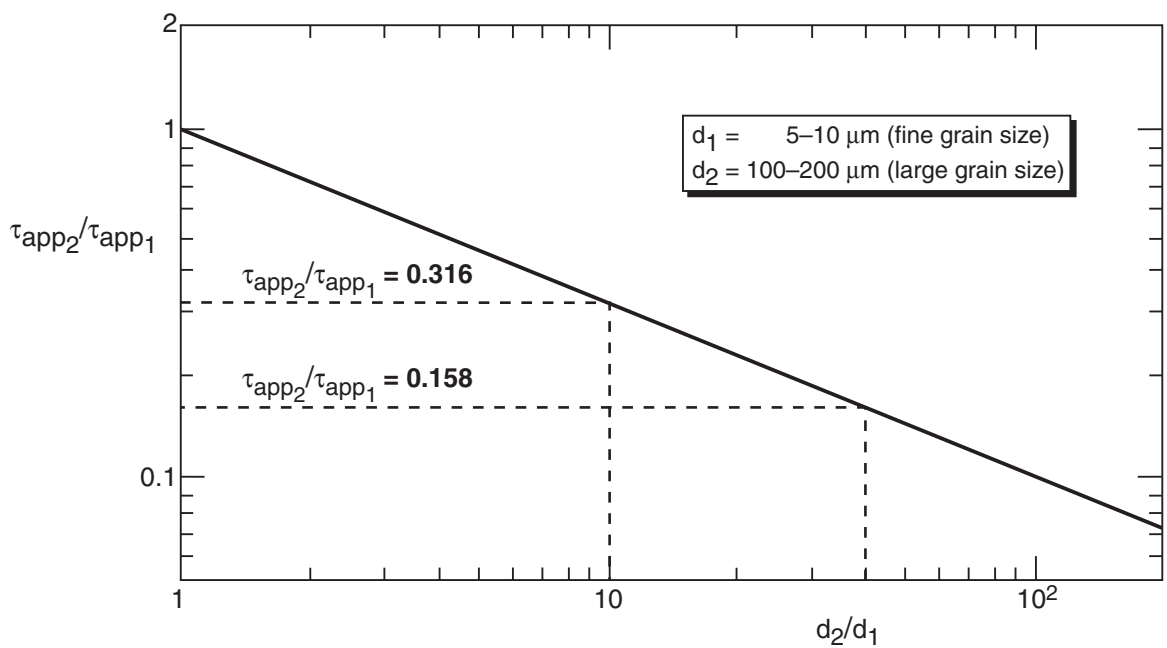

Fig. B.8   Dimensionless plot of the applied shear stress, τ_{app}, versus average grain diameter, d, using the proportionality $\tau_{app} \propto \sqrt{1/d}$